Thermophoresis in Dispersed Nanoparticle

Udit Sharma, Jeffrey S. Allen

QUICK LINKS

Abstract

This study explores the complex interplay of factors influencing thermal conductivity enhancement in nanofluids, which are suspensions of nanoparticles in base fluids. Nanofluids have emerged as promising materials for improving thermal properties due to the high thermal conductivity of certain nanoparticles. The research delves into the phenomenon of thermophoresis, considering temperature-dependent properties of base fluids and nanofluids. It analyzes five particle materials (gold, alumina, titania, copper, and silver) and six types of base-fluids to understand particle migration potential. The study suggests that variations in scaled thermal diffusion factor with temperature and particle size indicate potential for more uniform particle distribution at higher temperatures and smaller sizes. Nanoparticle material and volume fraction also impact migration potential, with certain materials showing thermophoretic potential over wider temperature ranges. Additionally, the study investigates Kapitza resistance at the nanoparticle-fluid interface, which significantly affects effective thermal conductivity. Molecular dynamics simulations and experimental studies have calculated Kapitza resistance for various interfaces, highlighting its temperature-dependent nature. The study concludes by deriving a universal relationship between the Suratman number (Su) and the Scaled Thermal Diffusion Factor (ϕTS_T), providing insights into whether a system will develop a concentration gradient or remain uniformly distributed. This analysis serves as a valuable tool for predicting and designing nanofluid systems for enhanced thermal conductivity in various engineering applications.

keywords: Thermodynamics, Heat Transfer, Nanoparticles, Nanofluids, Thermophoresis, Thermal Conductivity Enhancement, migration, Kapitza Resistance, Interfacial Thermal Resistance

Version: 2
Date: Sunday 12th May, 2024
Contact: udits@mtu.edu

NOMENCLATURE

β	non-dimensional nanofluid thermal conductivity	(-)
c	concentration	(kg/m^3)
χ	ratio of nanolayer thickness to particle radius	(-)
D_B	Brownian diffusion coefficient	(m^2/s)
D_D	Dufour coefficient	(m^2/s-K)
d_p	particle diameter	(m)
D_T	thermodiffusion coefficient	(m^2/s-K)
ε	volume ratio for ellipsoid	(-)
f	subscript for base fluid	(-)
G	Kapitza resistance at solid-liquid interface	(W/m^2-K)
γ	nanolayer thermal conductivity to particle thermal conductivity	(-)
J_p	mass diffusive flux	(kg/m^2/s)
$J_{p,c}$	mass diffusive flux due to concentration gradient	(kg/m^2/s)
$J_{p,T}$	mass diffusive flux due to temperature gradient	(kg/m^2/s)
k_B	Boltzmann Constant	(m^2kg/s^2-K)
k_f	base fluid thermal conductivity	(W/m-K)
k_{nf}	nanofluid thermal conductivity	(W/m-K)
k_p	particle thermal conductivity	(W/m-K)
k_{pe}	equivalent particle thermal conductivity	(W/m-K)
l_p	particle length	(m)
μ_T	chemical potential	(J/kg)
μ_{nf}	viscosity of nanofluid	(N-s/m^2)
μ_f	viscosity of base fluid	(N-s/m^2)
nf	subscript for nanofluid	(-)
p	subscript for particle	(-)
ϕ	volume fraction of particles	(-)
ϕ_e	equivalent volume fraction of particles	(-)
Pr	Prandtl number	(-)
r_p	radius of particle	(nm)
ρ_f	density of base fluid	(kg/m^3)
ρ_{nf}	density of nano fluid	(kg/m^3)
ρ_p	density of nanoparticle	(kg/m^3)
S_T	Soret Coefficient	(K^{-1})
Su	Suratman Number	(K^{-1})
Su^*	Critical Suratman Number	(K^{-1})
σ^*	interaction energy	(N/m)
T	temperature	(K)
T_m	melting temperature	(K)
V_T	drift velocity	(m/s)

1. Introduction

Thermal management is a critical aspect in numerous engineering applications, from electronics cooling to solar thermal energy conversion. Traditional heat transfer fluids, while effective, often possess limitations in their ability to conduct heat efficiently. In this regard, nanofluids have emerged as a promising class of engineered materials with the potential to revolutionize thermal management strategies. Nanofluids are suspensions of nanoparticles, with diameters typically ranging from 1-100 nanometers, dispersed in a base fluid such as water, ethylene glycol, or oil[1]. The burgeoning field of nanotechnology has ushered in a new era of material design, with nanofluids standing as a prime example. These suspensions of nanoparticles in base fluids offer the tantalizing prospect of significantly enhanced thermal properties, particularly thermal conductivity. The key innovation lies in the exploitation of the exceptionally high thermal conductivity of certain nanoparticles, such as metals, carbon nanotubes, or metal oxides. By incorporating these nanoparticles into the base fluid, researchers have observed significant enhancements in the overall thermal conductivity of the resulting nanofluid[2–4].

Researchers have explored the mechanisms by which nanoparticles enhance thermal conductivity in nanofluids. Factors such as nanoparticle material, size, concentration, temperature and base fluid properties influence thermal conductivity [5]. However, accurately measuring thermal conductivity in nanofluids presents unique challenges due to their size-dependent behavior and potential instabilities, requiring diverse measurement techniques. Contact methods offer direct interaction but can introduce disturbances, while non-contact techniques provide a more pristine approach[6].

The improved thermal conductivity of nanofluids is attributed to ballistic transport, enhanced Brownian motion, and direct interactions among nanoparticles and with the base fluid. The volume fraction of nanoparticles is a crucial parameter influencing thermal conductivity, generally increasing with increasing volume fraction but not always linearly due to agglomeration effects [2, 7–11]. Temperature also impacts thermal conductivity, affecting Brownian motion, base fluid properties, and nanoparticle properties, necessitating careful consideration in nanofluid design. Discrepancies in experimental measurements are attributed to measurement techniques, nanoparticle characteristics, base fluid properties, and temperature variations, highlighting the need for standardized protocols and detailed characterization.

Moreover, these discrepancies in published results contribute to the absence of a robust model that can elucidate the physics underlying this en-

hancement [12–15]. Evans et al. [16] demonstrated that effective medium theory can predict this enhancement without considering the effect of Brownian diffusion, contrasting with Choi [13] who argued that Brownian motion governs the thermal behavior of nanofluids. Eastman [17] proposed ballistic transport as the reason for thermal conductivity enhancement, while J. A. Eastman and Keblinski [18] identified particle size, agglomeration, particle-fluid interface, and temperature as major contributors. Viscosity and other thermophysical properties can also significantly influence heat transfer enhancement [19, 20]. Experimental observations, such as those by Gao [10], show that thermal conductivity is higher at higher temperatures for certain nanofluids, but Ho and Gao [21] reported reduced enhancement with increased nanoparticle mass fraction due to reduced convection . The enhancement in thermal conductivity is experimentally observed to be temperature dependent, Gao [10] showed that thermal conductivity was higher at higher temperature for the nanofluid made from n-Octadecane and Alumina. Ho and Gao [21] reported a lower heater enhancement with the increased nanoparticle mass fraction due to reduced convection. [22–25] suggest that Brownian motion plays a dominant role in thermal conductivity enhancement, while others argue that it only affects nanoparticles and not heat transfer [26, 27]. When particles are introduced into a base fluid, they exhibit random movement known as Brownian motion. This motion helps maintain a uniform concentration within the system, counteracting the formation of concentration gradients. However, when a temperature gradient is applied to the nanofluid, a phenomenon called thermophoresis occurs. Thermophoresis causes particles to move towards the colder regions of the system, contrary to the action of Brownian diffusion. The interplay between these two processes can lead to either a uniform distribution of particles or a non-uniform distribution, with particles potentially migrating towards the colder regions. This dominant mode of diffusion is determined by a thermal diffusion factor, a dimensionless number that characterizes the prevailing mode between Brownian and thermal diffusion. The discrepancies observed in experimental results regarding the enhancement of thermal conductivity in the base fluid could be attributed to this particle migration phenomenon.

2. Thermophoresis

The motion of particle due to the presence of temperature gradient, on top of Brownian motion is known as thermophoresis. Predominantly, the motion of particle occurs from the hot region towards the cold end [28]. The diffusion defined by Fick's equation relates the flux of particles/mass due to the concentration gradient. Heat transfer and nanoparticle trans-

port are thermodynamically coupled.

$$\text{heat flux} \quad J_q = -\mu_T T D_D \frac{dc}{dx} - k\frac{dT}{dx} \tag{1}$$

$$\text{particle flux} \quad J_p = -D_B \frac{dc}{dx} - cD_T \frac{dT}{dx} = J_{p,c} + J_{p,T} \tag{2}$$

The transport forces are thermal (T) and chemical (μ_T) [29–33]. D_B is Brownian diffusion coefficient,D_T is Thermal diffusion coefficient, D_D is the Dufour coefficient, c is concentration of particles,μ_T is chemical potential, k is the thermal conductivity, $J_{p,c}$ and $J_{p,T}$ are the diffusion flux due to concentration and temperature gradient respectively. Thus, the transport of particles can result from the combination of two factors: temperature gradient and concentration gradient. Mechanisms such as sedimentation or buoyancy are not considered here. The thermophoretic motion of particles occurs on top of the Brownian diffusion, though there is no external field is present [34]. The velocity attained by particles due to themrophoresis is called drift/thermophoretic velocity[35].

$$V_T = -D_T \frac{dT}{dx} \tag{3}$$

By experimental verification, it was found that this thermophoretic velocity in liquid is the modification of the Epstein's relation and is given by [36] [2] [37]

$$V_T = -\beta \frac{\mu_{nf}}{\rho_{nf}} \frac{1}{T} \frac{dT}{dx} \quad , \quad \beta = 0.26 \frac{k_f}{2k_f + k_p} \tag{4}$$

μ_{nf} is the viscosity of the nanofluid, ρ_{nf} is the density of nanofluid , k_{nf} and k_p are the thermal conductivity of nanofluid and particle respectively. We are using the term nanofluid for the combination of base fluid dispersed with some fraction of nano particles.

The relative strength of Brownian diffusion and thermal diffusion can be evaluated at zero net mass flux [38]

$$\text{at } J_p = 0 \quad , \quad \frac{1}{c}\frac{dc}{dx} = -\frac{D_T}{D_B}\frac{dT}{dx} \quad \text{where} \quad S_T = \frac{D_T}{D_B} \tag{5}$$

Soret coefficient S_T is the ratio between the thermal diffusion coefficient and the Brownian diffusion coefficient, with the units of K^{-1}.
Comparing 2 and 3, we can find that D_T is Thermal diffusion coefficient is given by

$$D_T = \frac{\beta}{\rho_{nf}} \frac{\mu_{nf}}{T} = 0.26 \frac{k_f}{2k_f + k_p} \frac{\mu_{nf}}{\rho_{nf} T} \tag{6}$$

Experiments suggests thermal diffusion coefficient varies between $1 * 10^{-8} < D_T < 1 * 10^{-7} cm^2 s^{-1} K^{-1}$ [39].
Brownian diffusion coefficient D_B is given by Stokes-Einstein equation [40]

$$D_B = \frac{k_B T}{3\pi \mu_f d_p} \tag{7}$$

From 6 and 7 we find

$$\text{Soret Coefficient} \quad S_T = \frac{3\pi \mu_{nf} \mu_f d_p \beta}{\rho_{nf} k_B T^2} \tag{8}$$

d_p is particle diameter, μ_f is the viscosity of the base fluid, ρ_p is the density of particle, k_B is Boltzmann constant.

The relative effect of the thermal diffusion to the Brownian diffusion can be written in the non-dimensional form by multiplying Soret coefficient by temperature. This is known as thermal diffusion factor.

$$TS_T = -\left(\frac{\frac{1}{c}\frac{\partial c}{\partial x}}{\frac{1}{T}\frac{\partial T}{\partial x}} \right)_{J_p=0} = \frac{3\pi \mu_{nf} \mu_f d_p \beta}{\rho_{nf} k_B T} \tag{9}$$

The expected value from the above relation aligns with the values provided by Würger [41]. The equation 9 do not account for the volume fraction ϕ of the particles in the basefluid. In order to capture the effect, thermal diffusion factor is multiplied by ϕ to get a scaled non-dimensional parameter ϕTS_T.

$$\phi TS_T = \phi \frac{3\pi \mu_{nf} \mu_f d_p \beta}{\rho_{nf} k_B T} \tag{10}$$

This scaled thermal diffusion factor will determine determine the dominant diffusion effect. When $\phi TS_T < 1$, Brownian diffusion prevents the development of a nanoparticle concentration gradient . When $\phi TS_T > 1$, then a nanoparticle concentration gradient might develop due to thermophoresis. It can be seen from the above equations that scaled thermal diffusion factor and the properties responsible for particle diffusion are temperature dependent. Thus, we can not assume the properties to be constant over the applicable range of temperature. So it is necessary to provide these properties as a function of temperature and it is shown in table 1.

2.1. Scaled Thermal Diffusion Factor

It can be seen from the equation above 9 that ϕTS_T is a function of

- Density of nanofluid

Version: 2
Date: Sunday 12th May, 2024
Contact: udits@mtu.edu

Table 1: Temperature dependent properties [42–45]

	Ethylene Glycol	Water	Acrylic Acid	Formic Acid	Caprylic Acid	Acetic Acid	Paraffin Wax
Density, $[g/mL]$, $AB^{-(1-T/T_c)^n}$							
A	0.32503	0 .34710	0.34645	0.36821	0.29231	0.35182	0.23837
B	0.25499	0.27400	0.25822	0.24296	0.26676	0.26954	0.25763
n	0.172	0.28571	0.30701	0.23663	0.28020	0.26843	0.274
T_c, K	645	647.13	615	580	692	592.71	745.26
Viscosity, $[cp]$,$\log_{10}\mu = A + B/T + CT + DT^2$							
A	-16.9728	-10.2158	-15.9215	-4.2125	-10.4823	3.8937	-8.5505
B∗10^3	3.1886	1.7925	2.4408	0.97953	2.067	.784	1.6708
C∗10^{-2}	3.2537	1.7730	3.4383	0.552	1.8423	0.6665	1.5675
D∗10^{-5}	-2.448	-1.2631	-2.7677	-0.57723	-1.3722	-0.75606	-1.2341
Thermal Conductivity, [W/m-K], for organic compound $\log_{10} K = A + B\left(1 - \frac{T}{C}\right)^{\frac{2}{3}}$, for inorganic $K = A + BT + CT^2$							
A	-0.5918	0.2758	-1.6101	-0.8626	-1.6624	-1.2836	-1.5198
B	-	4.61E-03	0.9742	0.3692	0.9819	0.5893	0.8067
C	645	-5.5391E-06	615	580	692	592.71	745.26
Specific Heat, $[J/mol - K]$,$C_p = A + BT + CT^2 + DT^3$							
A	75.878	92.053	-18.242	-16.110	70.790	-18.944	151.154
B	6.4182E-01	-3.9953E-02	1.2106	8.7229E-01	1.7647	1.0971	2.7878
C∗10^{-3}	-1.6493	-0.21103	-3.1160	-2.3665	-4.1521	-2.8921	-6.1542
D∗10^{-6}	1.6937	0.53469	3.1409	-2.4454	3.9451	2.9275	5.5249

- Viscosity of basefluid and the nanofluid
- Thermal conductivity of the nanofluid and the particles
- Diameter of dispersed nanoparticles
- Temperature
- Volume fraction of particles

3. Concept Discussion and Results

It has been discussed that there are several experimentally validated relations for predicting the thermal conductivity, Brownian diffusion coefficient and thermal diffusion coefficient. But none has combined the results of all the fields in one analysis and tried to capture the impact of temperature and its gradient on the migration of particles in the nanofluids. In order to provide the in-depth analysis on thermophoresis we have captured the temperature dependent properties of the basefluid as well as nanofluid.

Five particle materials were included in this study: gold, alumina, titania, copper and silver. The density and thermal conductivity for these particles are listed in Table 2. These properties are considered constant as the variation in density and thermal conductivity for the particle is insignificant within the applicable temperature range.

Table 2: Properties of Nanoparticles [42, 45]

	Density [kg/m^3], ρ_p	Thermal Conductivity [W/m-K], k_p
Alumina	3950	50
Copper	8960	402
Gold	19300	317.422
Silver	10500	428.227
Titania	4000	11.7

Six types of PCMs were studied. These were modeled only in the liquid phase without solidification. The base fluids are acetic acid, acrylic acid, caprylic acid, ethylene glycol, formic acid and water. Nanoparticles of the five materials listed earlier were paired with these fluids with varying particle size and volume fraction. The potential for particles to migrate or to remain uniformly distributed depends on the size of nanoparticles, volume fraction, particle type, fluid, and operating temperature range.

3.1. Impact of Temperature and Particle Size

Variations in thermal diffusion factor with temperature for copper particles of diameter 5 and 20 nm at 3% volume fraction in all six fluids are shown in Fig 1b and Fig 1c. Another data for several experiments conducted using various fluid and particle combination is shown in Fig 1a. It can be seen from these figures, that particles are expected to be more uniformly distributed at higher temperatures and thus, the migration towards cold end. This result is supported by experimental and molecular dynamic simulation results of Galliero and Volz [46], Duhr and Braun [47]. This can be attributed to the lower viscosity of fluid at higher temperature, resulting in better mobility of particles and more impact of Brownian diffusion. When we observe Fig 1b and Fig 1c we see that there is dependency of particle distribution on its size. $_T$ curve shifts towards the non-uniform zone when particle size changes from 5 nm to 20 nm. The depiction from the figures suggests that bigger particles are expected to be more non-uniformly distributed and towards the cold end. This observation aligns with the results reported by Lüsebrink and Ripoll [48].

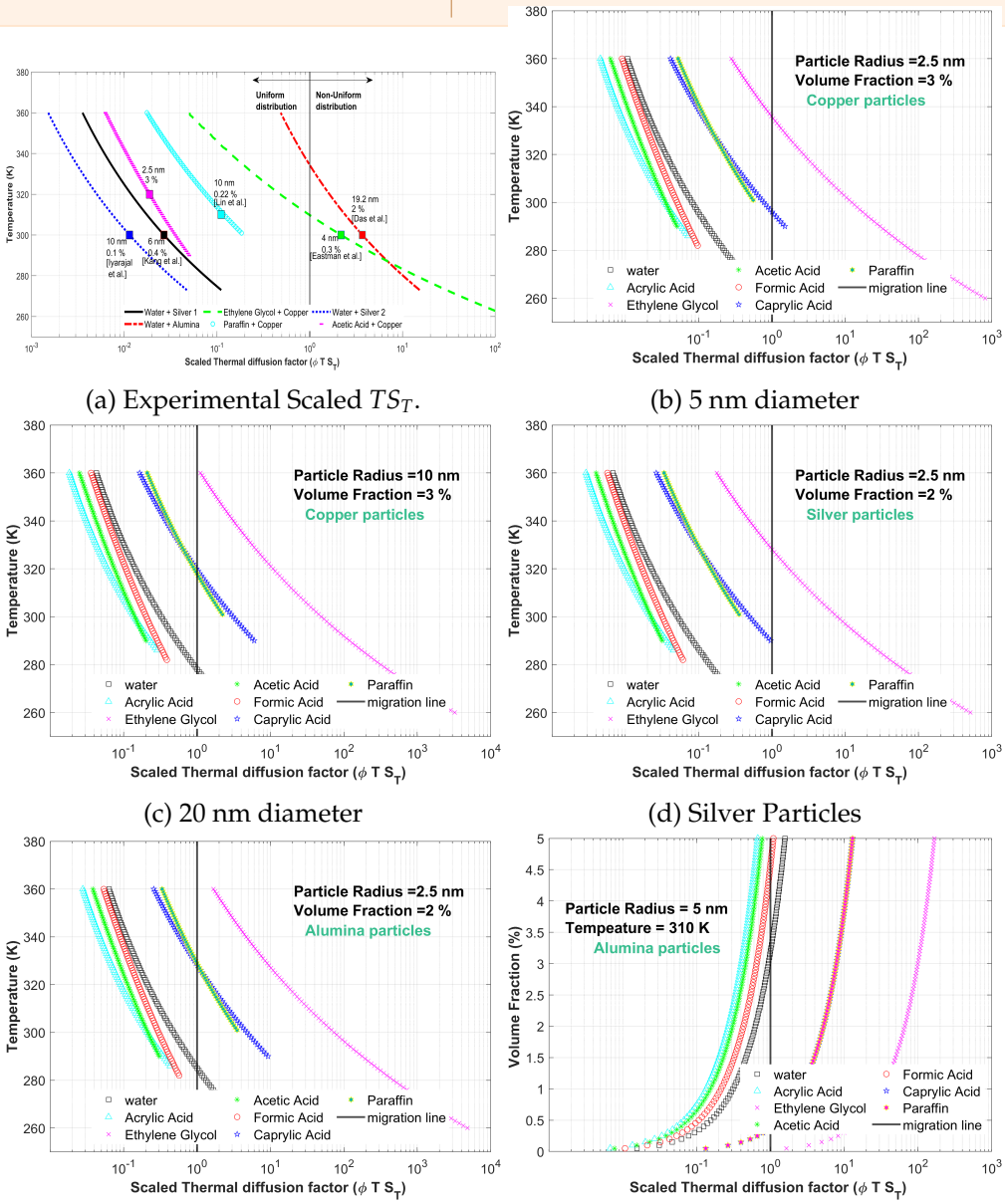

(a) Experimental Scaled TS_T.

(b) 5 nm diameter

(c) 20 nm diameter

(d) Silver Particles

(e) Alumina Particles

(f) ϕTS$_T$ vs volume fraction

Figure 1: Scaled thermal diffusion factor dependency on various parameters

3.2. Impact of Particle Material

Nanoparticles of alumina and silver with a diameter of 5 nm and a volume fraction of 2% were investigated. Alumina particles (Fig 1e) exhibited potential for thermophoresis across all temperature ranges. In contrast, for temperatures exceeding 300 K, Brownian diffusion dominated for silver particles (Fig 1d) dispersed in water, acrylic acid, formic

acid, and acetic acid.

The differences in thermal conductivity among various particle types influenced their migration behavior. Alumina, having a relatively low thermal conductivity compared to silver, showed this effect. This trend was also observed for other particles with lower thermal conductivity, such as Titania, while particles with higher thermal conductivity, like gold and copper, exhibited potential for uniform distribution. However, the impact of particle density on migration was minor, as the addition of nanoparticles minimally altered nanofluid density, which changes proportionally with particle fraction. Hence, fluid density primarily determined nanofluid density. The findings suggest that to compensate for the lower thermal conductivity of alumina and achieve equivalent thermal diffusion to silver, its density would need to increase by 120 times.

3.3. Impact of Volume Fraction

The effect of volume fraction is shown in Fig 1f. The graph illustrates the change in the scaled thermal diffusion factor for volume fractions up to 5% using only alumina particles at 310 K as an example. Similar results are observed for other particle types and temperatures. However, an intriguing observation is evident. At lower volume fractions, particles are expected to be uniformly distributed. As the volume fraction increases, there is a tendency for particles to create a concentration gradient. Another observation is that at lower volume fraction of particles, the change in ϕTS_T is steeper but with the increased volume fraction, it becomes less sensitive. This suggests that there exists an optimal volume fraction of particles that should be added to achieve uniform distribution and consequently, the maximum enhancement in thermal conductivity. Further discussion on the relationship between thermal conductivity enhancement and particle distribution will be presented in the following section.

3.4. Comparison with Reported Published Data

Figure 1a illustrates the trends in ϕTS_T for selected particle-fluid pairs, alongside test conditions from studies on enhancing thermal conductivity in phase change materials [1, 5, 14, 49, 50]. The data from Iyahraja1 and Rajadurai [49] and Kang et al. [1] (black and blue symbols, respectively) align with predicted trend lines, suggesting a strong impact of increasing volume fraction from very low concentrations on enhancing thermophoretic migration. Despite silver particles with a 10 nm diameter (blue square) and a 0.1% volume fraction, another data point (black square) shifts towards the non-uniformity zone due to a slightly higher 0.4% volume fraction of particles. Additionally, the use of lower thermal

conductivity particles like alumina, as indicated by the red square [5], results in a shift towards higher thermophoretic potential. Fluid viscosity, represented by the dashed green trend line, significantly influences particle migration, as seen in test conditions from Eastman et al. [14] (green square). The commonly used phase change material (PCM), paraffin, shows that dispersing copper nanoparticles with a 10 nm radius may lead to thermophoretic migration [50].

The experimental data suggests that concentration gradients can either build up or be uniformly distributed depending on the fluid and nanoparticle pairing. However, the most significant observation is that higher enhancements in thermal conductivity of nanofluids occur when ϕTS_T is less than 1, indicating uniform distribution. A thermal conductivity enhancement of 54%, 10%, and 24% respectively was measured by Kang et al. [1], Iyahraja1 and Rajadurai [49], Lin and Al-Kayiem [50], all lying in the uniform distribution zone. In contrast, the measured enhancement by Das et al. [5], Eastman et al. [14] was 4%, and both their data points lie in the non-uniformity zone. For instance, experiments by Lin and Eastman both using copper nanoparticles show one in the uniform region while the other in the non-uniform region. This disparity is attributed to variations in fluid type, particle size, and operating temperature. If the experiment by Eastman (represented by the green square) were conducted at 310 K instead of 300 K, the point would shift towards uniform distribution, potentially increasing the observed enhancement in thermal conductivity. This observation of non-uniform distribution of particles impacting the enhancement in the nanofluid aligns with the findings of Ding and Wen [51], Bahiraei and Hosseinalipour [52]. Additionally, returning to Figure 1a, it is evident that the addition of nanoparticles at lower concentrations could significantly increase thermal conductivity, but as the volume fraction of particles increases, the impact lessens, and the concentration gradient begins to build up. This is also supported by Buongiorno et al. [53], who found that adding 22 nm silica particles to water with a 31% volume fraction had almost no impact on thermal conductivity.

4. Interfacial Interaction Energy and Kapitza Resistance

Kapitza resistance, also known as interfacial thermal resistance or thermal boundary resistance, is a phenomenon that occurs at the interface between a solid and a liquid. It describes the resistance to heat flow across this interface, resulting in a temperature discontinuity or drop. The origin of Kapitza resistance lies in the mismatch between the vibrational properties of the solid and the liquid. When heat flows from the

solid to the liquid, the energy carriers must undergo scattering at the interface due to the differences in their vibrational spectra and velocities. The presence of Kapitza resistance at the nanoparticle-fluid interface can significantly influence the effective thermal conductivity of nanofluids. While the addition of nanoparticles is intended to enhance the thermal conductivity, the interfacial resistance can counteract this effect by impeding heat transfer between the nanoparticles and the base fluid. We define the interaction (σ^*) energy between the solid-liquid interface using the Kapitza resistance.

$$\sigma^* = \frac{G.A}{D_T} \tag{11}$$

G is the Kapitza conductance (inverse of Kapitza resistance) of the solid-liquid interface and A is the surface area of the particle. G is $O(10^8)$.Kapitza resistance is influenced by nanoparticle size, nanoparticle-fluid interaction and nanoparticle concentration. The book on nanofins [54], discusses the impact of fluid and the fin material to enhance the boiling. It shows that though the thermal resistance of silicon nanowires is higher than CNTs but the total thermal resistance in a circuit is lower due to substantially low interfacial thermal resistance. The book also discusses that precipitation of the nanoparticles act as the nanofins and can enhance the heat transfer, but excessive precipitation can have the negative impact on it.

The article by Khodayari et al. [55] employs molecular dynamics simulations to investigate the Kapitza resistance between nanoparticles and solid surfaces. The key findings reveal that the presence of nanoparticles near the solid-liquid interface increases the Kapitza resistance, hindering heat transfer from the solid surface to the liquid. The nanoparticles contribute significantly to the reduction in heat current, and their dynamics coupled with the solid surface lead to a shift in the major heat carriers from low to higher frequencies. The study explores realistic and simplified molecular models, varying nanoparticle-nanoparticle and nanoparticle-surface interactions, and employs the thermal relaxation method to determine the interfacial thermal conductance between the nanoparticle-containing suspension and the gold surface. Another work by Dolatabadi et al. [56] presents a comprehensive model for predicting the thermal conductivity of nanofluids, accounting for various factors that influence heat transfer at the nanoscale. The model incorporates the Kapitza resistance (interfacial thermal resistance) between nanoparticles and the base fluid, which can hinder heat transfer. It also considers the formation of a nanolayer around the nanoparticles, which can either enhance or reduce thermal conductivity depending on its properties. Additionally, the model includes the effects of convective diffusion due

to Brownian motion of nanoparticles and surface energy with capillary condensation, which can alter the surface properties and thermal conductivity. The thickness of the nanolayer is predicted using the BET isotherms and micro/nano-menisci generated pressures. The model is evaluated for four different nanofluids, and the results show good agreement with experimental data, providing a comprehensive framework for understanding and accurately predicting the thermal conductivity enhancement in nanofluids for heat transfer and thermal management applications.

Pollack [57], Ghasemi and Ward [58], Puech et al. [59] studied the kapitza resistance between the interface of liquid helium and various materials like copper, lead, silver, gold etc was calculated experimentally and it was found that $R_k \propto T^-3$. The generalized equation for kapitza resistance for a dispersed nanoparticle in a fluid is

$$R_k = \frac{15\hbar^3 \rho_p {c_t}^3}{16\pi^5 K_B^4 \rho_{bf} c_{bf} F \frac{c_l}{c_t} T^3} \tag{12}$$

where, $\hbar$, K_B, ρ_p, c_l, c_t and c_{bf} are the reduced Planck constant, Boltzmann constant, density of nanoparticle, longitudinal speed of sound in particle, transverse speed of sound in particle, and speed of sound in the base fluid respectively. Function, F, usually varies between 1.5 and 2.0[56, 57]. Interfacial resistance for various nanofluids like alumina and water, alumina and ethylene glycol and copper-oxide and water was calculated and it was found to vary between $0.5 * 10^{-8}$ to $1.86 * 10^{-8}$ m^2K/W [56]. Molecular dynamics simulation study also shows that there is a temperature jump across the solid-liquid interface and is characterized by interfacial resistance and kapitza length [60]. Equilibrium and Non-equilibrium molecular dynamic simulation for the water-graphene interface showed that R_k varies between $1.2 * 10^{-8}$ to $1.45 * 10^{-8}$ m^2K/W [61]. Another molecular dynamic simulation study showed that R_k is $O(10^{-8})$ for the silver nanoparticle in water. It also discusses that the heat is dissipated across a 2nm interfacial layer into water [62]. Experimental results have been compared with the Effective Medium Theory to predict the kapitza resistance, they were found to be in good agreement. The R_k for the alumina-water interface was $0.2 * 10^{-8}$ to $5 * 10^{-8}$ m^2K/W with a nanolayer thickness of 0.2 nm[55]. Review on nanoscale thermal transport by Cahill et al. [63] shows that kapitza conductance increases at higher temperature and is $O(10^8)$. This agrees with our analysis above in §3.1 that higher temperature operation tends to provide more uniform distribution of particles. The paper also discusses that the thermal conductance for gold and platinum nanoparticles is about $0.2 * 10^8$ to $1.3 * 10^8$ $Wm^{-2}K^{-1}$. A benchmark study performed by 30 organizations across the

globe to calculate the thermal conductivity of the nanofluids, using gold ,alumina and silica as the dispersion particles in water used the lower bond of R_k as 10^{-8} m^2K/W to justify their findings [53]. This shows that the validation of experiments needed a discrete value of kapitza resistance.

Singh et al. [64] used molecular dynamics simulations to study the thermal interfacial resistance between carbon nanotubes and different coolant fluids, including water, ethylene glycol, and a water-ethylene glycol mixture. The results showed that the thermal interfacial resistance was lowest for the water-based coolant, followed by the water-ethylene glycol mixture, and highest for pure ethylene glycol. This was attributed to the stronger water-carbon interactions in the water-based coolant, which led to a more ordered molecular layer at the interface and reduced the thermal resistance compared to the other coolants. The findings suggest that water-based nanofluids may be preferable as coolants compared to ethylene glycol-based fluids, due to the lower thermal interfacial resistance at the nanoparticle-fluid interface. The interfacial resistance was found to be $2.13 * 10^{-8}$, $4.74 * 10^{-8}$ and $7.29 * 10^{-8}$ m^2K/W for water, ethyl alcohol and 1-hexene respectively. Sarode et al. [65] investigates how the diameter of single-walled armchair carbon nanotubes (CNTs) affects the thermal interfacial resistance between the CNT and its surroundings. Using molecular dynamics simulations, the researchers found that thermal interfacial resistance decreases as CNT diameter increases, mainly due to the larger contact area provided by wider CNTs. For CNTs with diameters of a few nanometers, the total interfacial thermal conductance first decreases and then stabilizes as the number of walls increases, which is attributed to changes in mechanical strength and adhesive energy. They found that R_k varied between $0.7 * 10^{-8}$ and $2.6 * 10^{-8}$ m^2K/W. The book by Singh and Banerjee [54] compiles the data for over 25 fluid molecules and their isomers to show that R_k is $O(10^{-8})$ and it is strongly dependent on the solvent (basefluid).

5. Suratman Number Analysis

The temperature-dependent nature of properties such as viscosity, density, and thermal conductivity is evident in Equation 9. Monitoring the variation of each property with temperature individually would involve significant bookkeeping efforts to keep track of all the empirical relations. The distribution of particles has been shown to depend strongly on temperature, with the effect of temperature on ϕTS_T covering a wide range. Analyzing the data from this figure is challenging because the scaled thermal diffusion factor can vary widely with temperature. The curve can shift significantly to the left or right depending on the temperature-

dependent properties of the fluid and particles. Therefore, it would be advisable to use a more universal approach that can be applied to each particle-fluid combination.

Looking at the equation for the scaled thermal diffusion factor, Equation 9, we can see terms related to viscosity and inertia. Considering viscous and inertial forces along with the interaction between the solid-liquid interface, we can use the Suratman number (Su) for analysis. The Suratman number represents the ratio of surface tension forces to viscous forces in a fluid system. In nanofluids, it plays a crucial role in characterizing interfacial phenomena and flow behavior due to the presence of nanoparticles and their interactions with the base fluid. Su governs flow pattern transitions, pressure drop, and interfacial phenomena, making it essential for understanding and designing efficient two-phase flow systems, particularly in microfluidic and nanofluidic applications. Incorporating Su into theoretical models, correlations, and flow regime maps allows for a better understanding and prediction of the two-phase flow behavior of nanofluids, accounting for the effects of surface tension, viscosity, and nanoparticle-fluid interactions.

$$\text{Suratman Number,} \quad Su = \frac{\rho_{nf}\sigma^* d_p}{\mu_{nf}^2} \tag{13}$$

Here, Thus, the equation for Suratman number can be written as

$$Su = \frac{\pi G d_p^3 \rho_{nf}}{\mu_{nf}^2 D_T} \tag{14}$$

From 14 we see that Su already includes D_T in its mathematical representation. So analyzing thermal diffusion factor against Su will be easier and can yield some universal relationship.

5.1. Suratman Number vs Scaled Thermal Diffusion Factor

Based on the preceding discussion, we employed Equation 14 to derive a universal relationship between Su and ϕTS_T. The key parameters involved, namely the particle diameter, nanofluid density and viscosity, as well as the thermal diffusion coefficient, have been meticulously defined and elaborated upon in §2 and §3. Furthermore, the analysis of Kapitza resistance provides compelling evidence that the resistance (R_k) is of the order $O(10^{-8})$, or equivalently, the thermal conductance (G) is of the order $O(10^8)$. The values of G employed in our calculations are derived from Table 3. We conducted a comparison using gold and alumina particles, each with a diameter of 10 nm and a volume fraction of 2%, to plot Su versus ϕTS_T. The results are presented in Figure 2, indicating that data from

Table 3: Thermal Conductance of various Fluids

	Interfacial/Kapitza Conductance $[Wm^{-2}K^{-1}]$, G
Acetic Acid	$1 * 10^8$
Acrylic Acid	$1*10^8$
Caprylic Acid	$1.3*10^8$
Ethylene Glycol	$1*10^8$
Formic Acid	$0.8*10^8$
n-Octadecane	$1.3*10^8$
Water	$0.5*10^8$

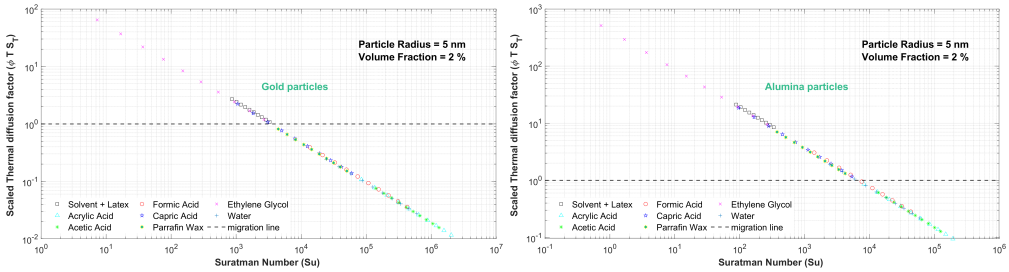

(a) Su vs Scaled TS_T for gold particles (b) Su vs Scaled TS_T for alumina particles

Figure 2: Comparison of Su vs Scaled Thermal Diffusion Factor for gold and alumina particles

various fluids collapses onto a single universal curve. This observation suggests a power law relationship, where the slope remains constant while the intercept varies depending on the fluid-particle pairing and their respective properties.

$$\phi TS_T = a * Su^b \tag{15}$$

In Equation 15, a represents the intercept, and b denotes the slope, where b is set to -0.68. We define the critical Suratman number (Su^*), as the point of intersection where $\phi TS_T = 1$. Data points to the left of Su^* are expected to exhibit non-uniform distribution, while those to the right should show uniform distribution. This analysis is crucial as it provides insight into whether the initial parameters will lead to the eventual development of a concentration gradient or if the particles will disperse uniformly.

To determine the alignment of the experimental points shown in Figure 1a with the predicted region, we have plotted all the experimental data points on the Su vs ϕTS_T curve. Two of them are illustrated in Figure 3:

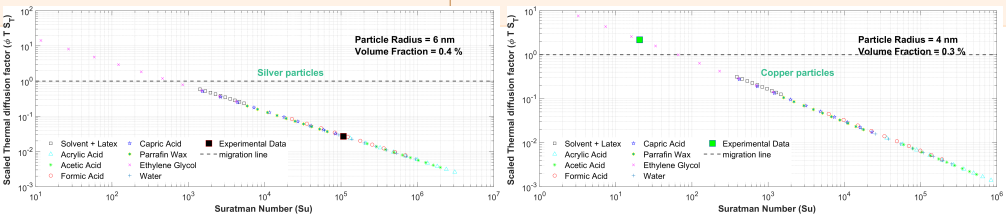

(a) Su vs Scaled TS_T for water silver 1 (b) Su vs Scaled TS_T for EG copper

Figure 3: Comparison of Su vs Scaled Thermal Diffusion Factor for experimental data points

in Figure 3b, the experimental data point lies to the left of Su^*, indicating non-uniform distribution, while the point in Figure 3a lies to the right of Su^*, suggesting the potential for a uniform distribution of particles. Please note that the symbol used to represent the experimental data points is similar to those used in Figure 1a, facilitating easy comparison between the two plots. Based on this plot, we can directly determine the critical Suratman number and ascertain whether the particle-fluid pairing being used positions the point to the left or right of this value. This can be achieved by compiling all the data for all properties as a function of the particle radius, volume fraction and particle thermal conductivity.

$$\phi TS_T = a * Su^b, \quad \text{for critical Su} \quad \phi TS_T = 1$$

$$Su^* = \left(\frac{1}{a}\right)^{1/b}, \quad \text{b is constant} \quad , a = f(r, \phi, k_p)$$

$$Su^* = 172 \sqrt{\frac{k_p^o}{k_p}} (\phi)^{\beta} \left(\frac{r}{r^o}\right)^{\eta}$$

k_p and k_p^o represent the particle thermal conductivity and reference thermal conductivity in $W/m-K$, respectively. For carbon nanotubes (CNTs), known for their exceptionally high thermal conductivity, k_p^o is set at 2000 $W/m-K$. The variables r and r^o denote the particle radius and the reference radius in nm, with r^o being 1 nm in this context.After conducting the analysis, the obtained values are $\eta = 4.4$ and $\beta = 1.4$. Consider the scenario depicted in Figure 3a, involving silver particles with a radius of 6 nm and a volume fraction of 0.4%. Using the relationship from Equation 16 and a thermal conductivity value for silver, $k_p = 428$ W/m-K, we calculate $Su^* = 434$, aligning with the line of intersection at $\phi TS_T = 1$. The experimental data point marked by a black square corresponds to a Suratman number of 1.07×10^5, exceeding Su^*, indicating it lies within the zone of uniform distribution.

A similar analysis can be applied to the case in Figure 3b, involving copper nanoparticles with a radius of 4 nm and a volume fraction of

0.3%. Using a thermal conductivity value for copper, k_p = 402 W/m-K, we determine Su^* = 50. However, the data point represented by a green square has a Suratman number of 20, below the critical Suratman number, placing it within the non-uniformity zone. By adjusting the particle radius to 3 nm, the new Su^* = 14, indicating a move to the zone of uniform distribution. This analysis can aid in predicting system behavior before experiments, offering insights into concentration gradient development.

One significant benefit of this analysis is its temperature independence, as all temperature-dependent properties are encapsulated in the coefficients for Su^*. Additionally, the relation remains independent of the fluid used, as fluid impact is accounted for through the Kapitza resistance, which exhibits minimal variation and incorporates the varying fluid-particle interaction effects in the coefficients.

6. Summary and Conclusion

The article delves into the importance of thermal management in engineering applications and the potential of nanofluids, suspensions of nanoparticles in a base fluid, to enhance thermal conductivity. It emphasizes how factors like nanoparticle material, size, concentration, temperature, and base fluid properties influence thermal conductivity enhancement. Standardized protocols and detailed characterization are highlighted as necessary to address discrepancies in experimental results. The interplay between Brownian motion and thermophoresis is discussed, impacting particle distribution and, consequently, thermal conductivity enhancement in nanofluids. Thermophoresis in nanofluids is analyzed considering temperature-dependent properties of both the base fluid and the nanofluid. Five particle materials (gold, alumina, titania, copper, and silver) and six types of phase change materials (PCMs) in various base fluids and nanoparticle pairings are examined to understand particle migration potential. The analysis indicates that particle material, size, volume fraction, and temperature are crucial in designing nanofluids for enhanced thermal conductivity. Higher temperatures and smaller particle sizes may lead to more uniform particle distribution, underscoring their importance in nanofluid design.

The article also discusses the significance of Kapitza resistance in understanding the interfacial interplay between the fluid and the solid nanoparticles. Kapitza resistance at the nanoparticle-fluid interface can significantly impact effective thermal conductivity. Molecular dynamics simulations and experimental studies have calculated Kapitza resistance for various interfaces, offering insights into heat transfer in nanofluids. The Suratman number analysis is presented as a tool to characterize

interfacial phenomena and flow behavior in nanofluids, aiding in predicting particle distribution patterns based on temperature gradients. The concept of the critical Suratman number provides a valuable tool for preparing experiments in advance, predicting whether the system will develop a concentration gradient or remain uniformly distributed. Determining the critical Suratman number for different particle sizes, volume fractions, and materials allows researchers to anticipate nanofluid behavior and design experiments accordingly. This understanding is crucial for optimizing nanofluid thermal properties for applications like thermal management and energy conversion.

References

[1] Hyun Uk Kang, Sung Hyun Kim, and Je Myung Oh. Estimation of thermal conductivity of nanofluid using experimental effective particle volume. *Exp. Heat Transfer*, 19:181–191, 2006. doi: 10.1080/08916150600619281.

[2] J. Buongiorno. Convective Transport in Nanofluids. *Journal of Heat Transfer*, 128(3):240–250, 08 2005. ISSN 0022-1481. doi: 10.1115/1.2150834. URL https://doi.org/10.1115/1.2150834.

[3] Davood Domairry Ganji and Amir Malvandi. *Heat Transfer Enhancement Using Nanofluid Flow in Microchannels*. Elsevier, 2016.

[4] S.A. Angayarkanni; John Philip. Review on thermal properties of nanofluids: Recent developments. *Adv. Colloid Interface Sci.*, 225:146–176, sep 2015.

[5] Sarit Kumar Das, Nandy Putra, Peter Thiesen, and Wilfried Roetzel. Temperature Dependence of Thermal Conductivity Enhancement for Nanofluids. *J. Heat Transfer*, 125:567–574, 2003. doi: 10.1115/1.1571080.

[6] *NANOSCALE THERMAL MEASUREMENTS NEW CHALLENGES AND NEW OPPORTUNITIES*, number 17, 2023. International Heat Transfer Conference.

[7] J. Wang; H. Xie; Z. Xin. Thermal properties of heat storage composites containing multiwalled carbon nanotubes. *J. Appl. Phys.*, 2008.

[8] J. L. Zeng; L. X. Sun; F. Xu; Z. C. Tan; Z. H. Zhang; J. Zhang and T. Zhang. Study of a pcm based energy storage system containing ag nanoparticles. *J. Therm. Anal. Calorim.*, 2007.

[9] Yu-Dong Liu; Yue-Guo Zhou; Ming-Wei Tong; Xiao-San Zhou. Experimental study of thermal conductivity and phase change performance of nanofluids pcms. *Microfluid Nanofluid*, 2009.

[10] C. J. Ho; J. Y. Gao. Preparation and thermophysical properties of nanoparticle-in-paraffin emulsion as phase change material. *Int. Commun. Heat Mass Transfer*, 2009.

[11] S. Wu, T. X. Li, T. Yan, Y. J. Dai, and R. Z. Wang. High performance form-stable expanded graphite/stearic acid composite phase change material for modular thermal energy storage. *Int. J. Heat Mass Transfer*, 102:733–744, 2016.

[12] Chan. Hee. Chon; Kenneth. D. Kihm; Shin Pyo. Lee. Empirical correlation finding the role of temperature and particle size for al2o3 nanofluid thermal conductivity enhancement. *Appl. Phys. Lett.*, 87:153107, 2005.

[13] Seok Pil Jang; U . S. Choi. Role of brownian motion in the enhanced thermal conductivity of nanofluids. *Appl. Phys. Lett.*, 84:4316, 2004.

[14] J. A. Eastman, S. U. S. Choi, S. Li, W. Yu, and L. J. Thompson. Anomalously increased effective thermal conductivities of ethylene glycol-based nanofluids containing copper nanoparticles. *Appl. Phys. Lett.*, 78(6):718–720, 2001. doi: 10.1063/1.1341218.

[15] Stephen. U. S. Choi ; J. A. Eastman. Enhancing thermal conductivity of fluids with nanoparticles. *ASME Intenational Mechanical Engineering Congress and Exposition*, nov 1995.

[16] William Evans, Jacob Fish, and Pawel Keblinski. Role of brownian motion hydrodynamics on nanofluid thermal conductivity. *Applied Physics Letters*, 88(9), 2006. doi: 10.1063/1.2179118.

[17] P. Keblinski; S. R. Phillpot; S. U. S. Choi; J. A. Eastman. Mechanisms of heat flow in suspensions of nano-sized particles (nanofluids). *Int. J. Heat Mass Transfer*, 2002.

[18] S.U.S. Choi J. A. Eastman, S. R. Phillpot and P. Keblinski. Thermal transport in nanofluids. *Annu. Rev. Mater. Res.*, 2004.

[19] J.M.Khodadadi; S.F.Hosseinizadeh. Nanoparticle-enhanced phase change materials (nepcm) with great potential for improved thermal energy storage. *Int. Commun. Heat Mass Transfer*, 2007.

[20] Jorge L. Alvarado; Charles Marsh; Chang Sohn; Gary Phetteplace; Ty Newel. Thermal performance of microencapsulated phase changematerial slurry in turbulent flow under constant heat flux. *Int. J. Heat Mass Transfer*, 2007.

[21] C.J. Ho and J.Y. Gao. An experimental study on melting heat transfer of paraffin dispersed with al2o3 nanoparticles in a vertical enclosure. *Int. J. Heat Mass Transfer*, 2013.

[22] J. Koo and C. Kleinstreuer. Impact analysis of nanoparticle motion mechanisms on the thermal conductivity of nanofluids. *Int. Commun. Heat Mass Transfer*, 2005.

[23] Ravi Prasher, Prajesh Bhattacharya, and Patrick E. Phelan. Thermal conductivity of nanoscale colloidal solutions (nanofluids). *Physical Review Letters*, 94(2), January 2005. ISSN 1079-7114. doi: 10.1103/physrevlett.94.025901. URL http://dx.doi.org/10.1103/PhysRevLett.94.025901.

[24] Chan Hee Chon, Kenneth D. Kihm, Shin Pyo Lee, and Stephen U. S. Choi. Empirical correlation finding the role of temperature and particle size for nanofluid (al2o3) thermal conductivity enhancement. *Applied Physics Letters*, 87(15), October 2005. ISSN 1077-3118. doi: 10.1063/1.2093936. URL http://dx.doi.org/10.1063/1.2093936.

[25] Mehdi Bahiraei. Particle migration in nanofluids: A critical review. *International Journal of Thermal Sciences*, 109:90–113, November 2016. ISSN 1290-0729. doi: 10.1016/j.ijthermalsci.2016.05.033. URL http://dx.doi.org/10.1016/j.ijthermalsci.2016.05.033.

[26] L. Xue; P. Keblinski; S. R. Phillpot; S.U.S. Choi and J. A. Eastman. Effect of liquid layering at the liquid-solid interface on thermal transport. *Int. J. Heat Mass Transfer*, 2004.

[27] A. R. Khaled and K. Vafai. Heat transfer enhancement through control of thermal dispersion effects. *Int. J. Heat Mass Transfer*, 2005.

[28] Minsub Han. Thermophoresis in liquids: a molecular dynamics simulation study. *J. Colloid Interface Sci.*, 2005.

[29] Adrian Bejan. *Advanced Engineering Thermodynamics*. Wiley, 4th edition, 2016.

[30] Signe Kjelstrup, Dick Bedeaux, and Eivind Johannessen. *Elements of Irreversible Thermodynamics for Engineers*. Academic Press, 2nd edition, 2006. doi: 10.1142/10286.

[31] Signe Kjelstrup and Dick Bedeaux. *Non-Equilibrium Thermodynamics of Heterogenous Systems*, volume 16 of *Series on Advances in Statistical Mechanics*. World Scientific, 2008. doi: 10.1039/9781849730983-00460.

[32] Signe Kjelstrup, Dick Bedeaux, Eivind Johannessen, and Joachim Gross. *Non-equilibrium thermodynamics for engineers*. World Scientific, 2010. doi: 10.1142/10286.

[33] P. Mazur S.R.De Groot. *Non-Equilibrium Thermodynamics*. Dover Books on Physics. Dover Publications, Newburyport, 2013. ISBN 9780486153506. Description based upon print version of record.

[34] R. Piazza. Thermophoresis: Moving particle with thermal gradient. *Soft Matter*, 2008.

[35] J Calvin Giddings, Paul M Shinudu, and Semen Nikolaevich Semenov. Thermophoresis of metal particles in a liquid. *Journal of colloid and interface science*, 176(2):454–458, 1995.

[36] G.S McNab and A Meisen. Thermophoresis in liquids. *Journal of Colloid and Interface Science*, 44 (2):339–346, 1973. ISSN 0021-9797. doi: https://doi.org/10.1016/0021-9797(73)90225-7. URL https://www.sciencedirect.com/science/article/pii/0021979773902257.

[37] Paul S. Epstein. On the theory of the radiometer. *Magazine for Physics*, 1929.

[38] A. Parola and R. Piazza. Particle thermophoresis in liquids. *The European Physical Journal E*, 2004.

[39] Roberto Piazza and Andrea Guarino. Soret effect in interacting micellar solutions. *Physical Review Letters*, 2002.

[40] Byron Bird; Warren E. Stewart and Edwin N. Lightfoot. *Transport Phenomena*. John Wiley and Sons, 1960.

[41] Alois Würger. Thermal non-equilibrium transport in colloids. 73(12):126601, 2010.

[42] Carl L. Yaws. Chemical properties handbook:physical, thermodynamic, environmental, transport, safety, and health related properties for organic and inorganic chemicals. Mcgraw-Hill, Quebecor/Kingsport, 1999.

[43] A. Kayode Coker PhD. *Ludwig's Applied Process Design for Chemical and Petrochemical Plants, Fourth Edition 1*. Gulf Professional Publishing, 4 edition, 2007. ISBN 075067766X; 9780750677660. URL libgen.li/file.php?md5=cd7fcfac4fc3bcd3ede63cb5367b4cfb.

[44] John P. O'Connell Bruce E. Poling, John M. Prausnitz. *The properties of gases and liquids*. McGraw-Hill Professional, 5 edition, 2000. ISBN 0070116822; 9780070116825; 9780071499996; 0071499997. URL libgen.li/file.php?md5=9e7ba45542da02693d509794b1c6e902.

[45] Don. W. Green ; Robert. H. Perry. *Chemical Engineer's Handbook*. The McGraw-Hill Companies, USA, 8 edition, 2008.

[46] G. Galliero and S. Volz. Thermodiffusion in model nanofluids by molecular dynamics simulations. *The Journal of Chemical Physics*, 128(6), February 2008. ISSN 1089-7690. doi: 10.1063/1.2834545. URL http://dx.doi.org/10.1063/1.2834545.

[47] Stefan Duhr and Dieter Braun. Why molecules move along a temperature gradient. *Proceedings of the National Academy of Sciences*, 103(52):19678–19682, December 2006. ISSN 1091-6490. doi: 10.1073/pnas.0603873103. URL http://dx.doi.org/10.1073/pnas.0603873103.

[48] Daniel Lüsebrink and Marisol Ripoll. Collective thermodiffusion of colloidal suspensions. *The Journal of Chemical Physics*, 137(19), November 2012. ISSN 1089-7690. doi: 10.1063/1.4767398. URL http://dx.doi.org/10.1063/1.4767398.

[49] S. Iyahraja1 and J. Selwin Rajadurai. Study of thermal conductivity enhancement of aqueous suspensions containing silver nanoparticles. *AIP Adv.*, 5(057103):1–8, 2015. doi: 10.1063/1.4919808.

[50] Saw C. Lin and Hussain H. Al-Kayiem. Evaluation of copper nanoparticles - paraffin wax compositions for solar thermal energy storage. *Sol. Energy*, 132:267–278, 2016. doi: 10.1016/j.solener.2016.03.004.

[51] Yulong Ding and Dongsheng Wen. Particle migration in a flow of nanoparticle suspensions. *powder Technology*, 2004.

[52] Mehdi Bahiraei and Seyed Mostafa Hosseinalipour. Particle migration in nanofluids considering thermophoresis and its effect on convective heat transfer. 574:47–54.

[53] Jacopo Buongiorno, David C Venerus, Naveen Prabhat, Thomas McKrell, Jessica Townsend, Rebecca Christianson, Yuriy V Tolmachev, Pawel Keblinski, Lin-wen Hu, Jorge L Alvarado, et al. A benchmark study on the thermal conductivity of nanofluids. 106(9), 2009.

[54] Navdeep Singh and Debjyoti Banerjee. *Nanofins: science and applications*. Springer, 2014.

[55] Ali Khodayari, Matteo Fasano, Masoud Bozorg Bigdeli, Shahin Mohammadnejad, Eliodoro Chiavazzo, and Pietro Asinari. Effect of interfacial thermal resistance and nanolayer on estimates of effective thermal conductivity of nanofluids. *Case studies in thermal engineering*, 12:454–461, 2018. doi: https://doi.org/10.1016/j.csite.2018.06.005. URL https://www.sciencedirect.com/science/article/pii/S2214157X18300108#section-cited-by.

[56] Nader Dolatabadi, Ramin Rahmani, Homer Rahnejat, and Colin P Garner. Thermal conductivity and molecular heat transport of nanofluids. *RSC advances*, 9(5):2516–2524, 2019. doi: 10.1039/C8RA08987F. URL https://pubs.rsc.org/en/content/articlehtml/2019/ra/c8ra08987f.

[57] Gerald L. Pollack. Kapitza resistance. URL https://journals.aps.org/rmp/abstract/10.1103/RevModPhys.41.48.

[58] Hadi Ghasemi and Charles Ward. Mechanism of sessile water droplet evaporation. In *APS March Meeting Abstracts*, volume 2012, pages Q36–012.

[59] L. Puech, B. Hebral, D. Thoulouze, and B. Castaing. Liquid-solid ^{4}he interface: Kapitza resistance. *J. Physics Lett.*, 43:809–814, 1982.

[60] Bo Hung Kim, Ali Beskok, and Tahir Cagin. Molecular dynamics simulations of thermal resistance at the liquid-solid interface. 129(17), 2008.

[61] Sobin Alosious, Sridhar Kumar Kannam, Sarith P Sathian, and BD Todd. Kapitza resistance at water–graphene interfaces. 152(22).

[62] Ali Rajabpour, Roham Seif, Saeed Arabha, Mohammad Mahdi Heyhat, Samy Merabia, and Ali Hassanali. Thermal transport at a nanoparticle-water interface: A molecular dynamics and continuum modeling study. *The Journal of chemical physics*, 150(11), 2019.

[63] David G Cahill, Paul V Braun, Gang Chen, David R Clarke, Shanhui Fan, Kenneth E Goodson, Pawel Keblinski, William P King, Gerald D Mahan, Arun Majumdar, et al. Nanoscale thermal transport. ii. 2003–2012. *Applied physics reviews*, 1(1), 2014.

[64] N Singh, VU Unnikrishnan, D Banerjee, and JN Reddy. Analysis of thermal interfacial resistance between nanofins and various coolants. 12(5):254–260.

[65] Ajinkya Sarode, Zeeshan Ahmed, Pratik Basarkar, Atul Bhargav, and Debjyoti Banerjee. A molecular dynamics approach of the role of carbon nanotube diameter on thermal interfacial resistance through vibrational mismatch analysis. 122:33–38, 2017.